HTML ABSTRACT • LINKS

Etching of porous and solid SiO_2 in $Ar/c\text{-}C_4F_8$, $O_2/c\text{-}C_4F_8$ and $Ar/O_2/c\text{-}C_4F_8$ plasmas

Arvind Sankaran[a)]
Department of Chemical and Biomolecular Engineering, University of Illinois, 1406 West Green Street, Urbana, Illinois 61801

Mark J. Kushner[b)]
Department of Electrical and Computer Engineering, University of Illinois, 1406 West Green Street, Urbana Illinois 61801

(Received 28 July 2004; accepted 24 October 2004; published online 27 December 2004)

$C\text{-}C_4F_8$-based plasmas are used for selective etching of high aspect ratio (HAR) trenches in SiO_2 and other dielectrics for microelectronics fabrication. Additives such as Ar and O_2 are often used to optimize the process. Understanding the fundamentals of these processes is critical to extending technologies developed for solid SiO_2 to porous SiO_2, as used in low-dielectric constant insulators. To investigate these issues, reaction mechanisms developed for etching of solid and porous SiO_2 in fluorocarbon plasmas and for etching of organic polymers in O_2 plasmas have been incorporated into a feature profile model capable of addressing two-phase porous materials. The reaction mechanism was validated by comparison to experiments for blanket etching of solid and porous SiO_2 in $Ar/c\text{-}C_4F_8$ and $O_2/c\text{-}C_4F_8$ plasmas using inductively coupled plasma reactors. We found that the blanket etch rates of both solid and porous SiO_2 had maxima as a function of Ar and O_2 addition to $c\text{-}C_4F_8$ at mole fractions corresponding to an optimum thickness of the overlying polymer layer. Larger Ar and O_2 additions were required to optimize the etch rate for porous SiO_2. Whereas etch stops occurred during etching of HAR features in solid and porous SiO_2 using pure $c\text{-}C_4F_8$ plasmas, Ar and O_2 addition facilitated etching by reducing the polymer thickness, though with some loss of critical dimensions. Mixtures of $Ar/O_2/c\text{-}C_4F_8$ can be used to manage this tradeoff. © *2005 American Institute of Physics*. [DOI: 10.1063/1.1834979]

I. INTRODUCTION

Fluorocarbon plasma etching of SiO_2 and low-dielectric constant (low-*k*) porous SiO_2 is an indispensable process during the manufacture of microelectronics integrated circuits.[1–4] The longevity of pattern transfer by fluorocarbon plasmas is in large part a result of the excellent selectivity which can be obtained between different materials such as SiO_2, Si, and Si_3N_4.[5,6] The choice of fluorocarbon plasmas used for these processes depends on the desired feature topology and selectivity. Fluorocarbon chemistries such as CF_4, C_2F_6, CHF_3, and $c\text{-}C_4F_8$ with additives such as H_2, O_2, Ar, CO, and N_2 have been used for such applications.[4,7,8] Etch mechanisms for Si, SiO_2, and Si_3N_4 in fluorocarbon plasmas are similar and proceed through the formation of an overlying fluorocarbon polymer layer. The polymer thickness varies from being the thinnest on SiO_2 to being the thickest on Si.[9] The thickness of the polymer layer regulates the delivery of reactants and activation energy from the plasma to the surface of the wafer, which in turn determines the etch rates. The consumption of the fluorocarbon polymer by the oxygen in SiO_2 and the nitrogen in Si_3N_4 results in thinner layers on those materials, producing higher etch rates relative to Si. As there are similarities in the reaction mechanisms and comparable polymer layer thicknesses for Si_3N_4 and SiO_2, highly selective etching of SiO_2 with respect to Si_3N_4 is more difficult to achieve than either SiO_2 or Si_3N_4 etching with respect to Si.[9] In this regard, selective etching of SiO_2 and Si_3N_4 has been achieved in $c\text{-}C_4F_8$ plasmas.[5]

Additives such as O_2, Ar, and CO regulate the magnitudes of the polymerizing, etching neutral and ion fluxes incident upon the wafer, and so aid in achieving the desired selectivity and feature topology. For example, the addition of Ar typically controls the ratio of the neutral flux to the ion flux principally by increasing the Ar^+ flux. O_2 and CO addition can reduce the thickness of the polymer by oxygen atom etching. These additives ultimately control the thickness of the polymer layer by regulating fluxes for polymer formation, ion activated polymer consumption, and fluorine atom etching of the polymer. The choice of fluorocarbon gas and additives therefore determines etch rates, selectivity, and maintenance of the critical dimensions of the feature.[4,9–11]

Understanding the complex gas phase and surface reaction mechanisms of $c\text{-}C_4F_8$ plasma etching has been the goal of many previous investigations in inductively coupled plasma (ICP) and magnetically enhanced reactive ion etching (MERIE) reactors, among others.[4,7,12–14] For example, Li *et al.* investigated the etching of Si, SiO_2, and photoresist in $Ar/O_2/c\text{-}C_4F_8$ plasmas.[4,7] They found that, in general, Ar addition to $c\text{-}C_4F_8$ plasmas increased the etch selectivities of SiO_2 to Si and SiO_2 to resist, while O_2 addition reduced both

a)Present address: Novellus Systems, 11155 SW Leveton Drive, Tualatin, Oregon 97062; electronic mail: arvind.sankaran@novellus.com
b)Author to whom correspondence should be addressed. Present address: Iowa State University, 104 Marston Hall, Ames, IA 50011–2151; electronic mail: mjk@iastate.edu

 © 2005 American Institute of Physics

Downloaded 29 Jan 2005 to 129.186.96.224. Redistribution subject to AIP license or copyright, see http://jap.aip.org/jap/copyright.jsp

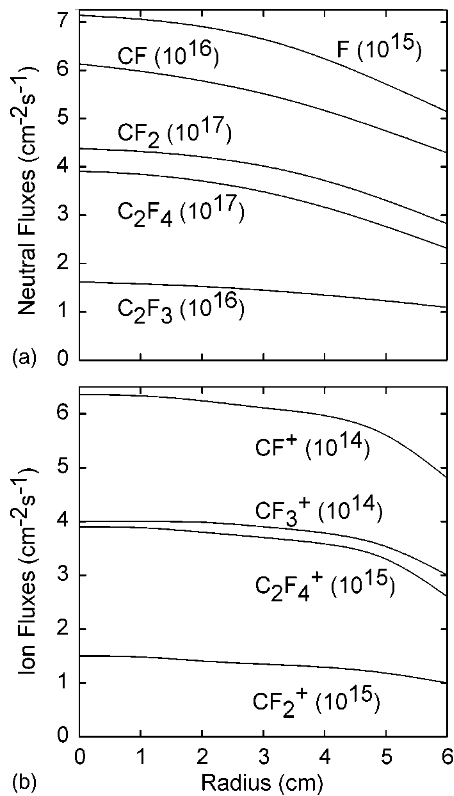

FIG. 1. Fluxes to the wafer as a function of radius for a c-C_4F_8 ICP plasma for the base case (c-C_4F_8, 20 mTorr, 40 sccm, 600-W ICP, −120-V self-bias). (a) CF_2, CF, C_2F_3, C_2F_4, and F. (b) CF^+, CF_2^+, CF_3^+, and $C_2F_4^+$. Due to the large power deposition, a significant dissociation of the feedback gas occurs.

selectivities. They found that the densities of CF_2 and CF were enhanced with small Ar addition, which they attributed to an increase in plasma density. Matsui *et al.* investigated the characteristics of the polymer layers formed on SiO_2, Si_3N_4, and Si in Ar/O_2/c-C_4F_8 plasmas.[5,9] They observed a 1-nm-thick polymer layer on SiO_2, whereas the thickness on Si_3N_4 and Si was ≈5–6 nm. These differences in polymer thickness explained the selectivity of the etching of SiO_2 to Si_3N_4 and SiO_2 to Si.

In this paper, we present results from a computational investigation of etching of solid and porous SiO_2 in Ar/c-C_4F_8, O_2/c-C_4F_8 and Ar/O_2/c-C_4F_8 plasmas using the Monte Carlo Feature Profile Model (MCFPM) which was modified to address two-phase porous materials. The MCFPM was coupled to the Hybrid Plasma Equipment Model (HPEM) which provided the energy and angular distributions of the reactants to the wafer. The surface reaction mechanisms previously developed for etching of solid and porous SiO_2 in pure fluorocarbon plasmas and the etching of organic polymers in O_2 plasmas were combined in this study.[15,16] Validation was accomplished by comparisons to experiments for blanket etch rates in ICPs for c-C_4F_8, Ar/c-C_4F_8, and O_2/c-C_4F_8 chemistries.[4]

Based on experimental comparisons, we found that Ar and O_2 additives to c-C_4F_8 control the thickness of the overlying polymer on SiO_2 and so regulate etch rates. Maxima in etch rates which occurred with increasing Ar or O_2 addition to c-C_4F_8 corresponded to obtaining an optimum polymer

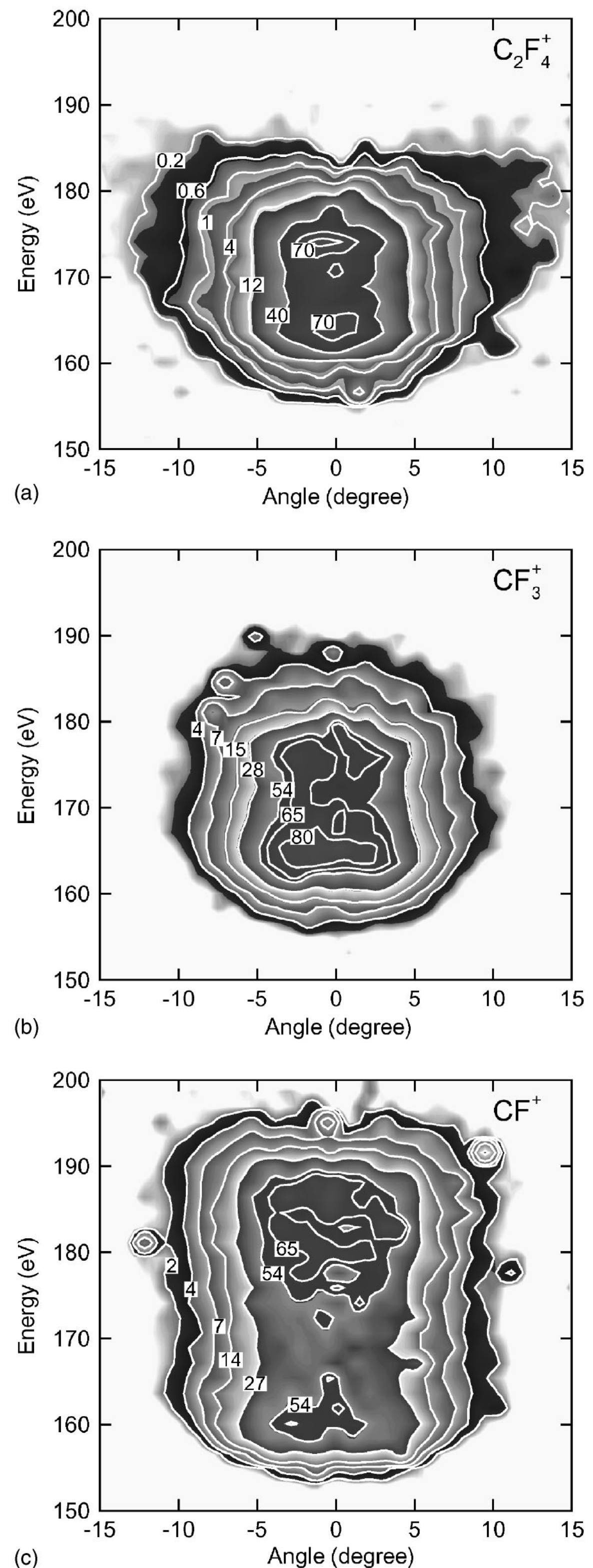

FIG. 2. Ion energy and angular distributions (IEADs) obtained with the Monte Carlo Plasma Chemistry Module incident on and averaged over the wafer for the base case (c-C_4F_8, 20 mTorr, 40 sccm, 600-W ICP, −120-V self-bias) for (a) $C_2F_4^+$, (b) CF_3^+, and (c) CF^+. The contour labels indicate the percentage of the maximum value. The IEADs for the heavier ions are narrower in both energy and angle.

layer thickness. Although for the conditions investigated, solid SiO_2 could be etched in pure c-C_4F_8, blanket etching of porous SiO_2 required the addition of Ar or O_2 to proceed due to the need to remove polymer from pores. Porous SiO_2 hav-

Downloaded 29 Jan 2005 to 129.186.96.224. Redistribution subject to AIP license or copyright, see http://jap.aip.org/jap/copyright.jsp

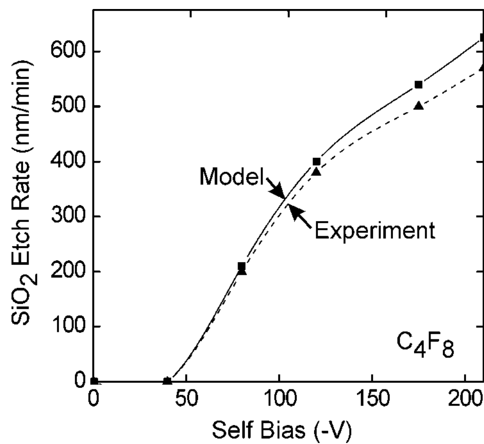

FIG. 3. A comparison of simulated and experimental results for solid SiO_2 etch rates as a function of self-generated dc bias voltage for a c-C_4F_8 plasma for the base case. Experimental results are from Ref. 4. Etching of SiO_2 has a threshold self-bias voltage of −40 V beyond which the etch rates increase as a function of the self-bias voltage.

ing larger pores and porosity required larger mole fractions of Ar or O_2 to optimize etch rates. Etch stop occurred during the evolution of high aspect ratio (HAR) trenches in solid SiO_2 due to sidewall polymer buildup. Ar and O_2 addition reduced the polymer thickness sufficiently to clear the feature, though smaller mole fractions of O_2 were required. In porous SiO_2, HAR features could not be cleared with Ar/c-C_4F_8, mixtures. O_2 addition was required.

The HPEM, the MCFPM, and the surface reaction mechanisms are discussed in Sec. II. Results for blanket etching of solid and porous SiO_2 in c-C_4F_8, Ar/c-C_4F_8, and O_2/c-C_4F_8 plasmas are presented in Sec. III. Examples of etching of HAR features in solid and porous SiO_2 in Ar/c-C_4F_8, O_2/c-C_4F_8, and Ar/O_2/c-C_4F_8 plasmas are presented in Sec. IV, followed by the concluding remarks in Sec. V.

II. DESCRIPTION OF THE MODELS

Reactor scale plasma properties were obtained from the HPEM which has been previously described and so is only briefly summarized here.[17,18] The HPEM is a two-dimensional (2D) simulator consisting of an electromagnetic module (EMM), an electron energy transport module (EETM), and a fluid kinetics module (FKM). Electromagnetic and magnetostatic fields are calculated in the EMM. These fields are then used in the EETM to obtain electron-impact source functions and transport coefficients by solving the electron energy equation. These results are then passed to the FKM, in which separate continuity, momentum, and energy equations are solved for ions and neutral species; and Poisson's equation is solved for the time varying electrostatic potential. Outputs from the FKM (densities and electrostatic fields) are transferred to EETM and EMM and the process is iterated until a converged solution is obtained. The gas phase reaction mechanism for Ar/O_2/c-C_4F_8 plasmas used in this investigation has also been previously described and validated, and is discussed in Ref. 19.

The Plasma Chemistry Monte Carlo Module (PCMCM) of the HPEM produces energy and angularly resolved distributions (EADs) for neutrals and ions striking the surface of the wafer which are then used by the MCFPM.[20] The PCMCM launches pseudoparticles representing ions and neutrals based on the electron-impact source functions obtained from the HPEM. Using a Monte Carlo simulation, the PCMCM integrates the trajectories of the ions and neutrals in the time varying electric field while capturing their gas phase collisions and interactions with the surface using the same reaction mechanism as in the HPEM. Statistics are collected on the energy and angle of the pseudoparticles as they strike specified locations on surfaces to produce time-averaged EADs.

The 2D MCFPM has also been previously described and so is briefly summarized here.[15,16,21] The MCFPM resolves the materials constituting the wafer and on the wafer using a 2D rectilinear mesh. Each cell in the mesh is assigned a material identity. Gas phase species are represented by pseudoparticles and surface species are represented by computational mesh cells. Pseudoparticles are launched towards the surface from random locations above the wafer with energies and angles sampled from the EADs obtained from the PCMCM. The trajectories of the pseudoparticles are tracked until they hit a surface, where a generalized surface reaction mechanism controls the interaction. The reaction mechanism

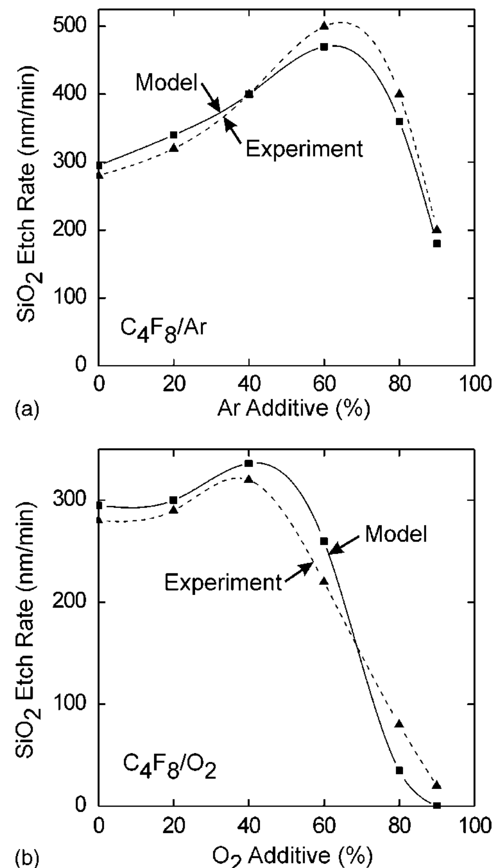

FIG. 4. A comparison of simulated and experimental results of SiO_2 etch rates as a function of (a) Ar and (b) O_2 mole fractions for the base case (c-C_4F_8, 20 mTorr, 40 sccm, −100-V self-bias). Experimental results are from Ref. 4. Addition of both Ar and O_2 reduces the polymer thickness and increases the etch rates.

Downloaded 29 Jan 2005 to 129.186.96.224. Redistribution subject to AIP license or copyright, see http://jap.aip.org/jap/copyright.jsp

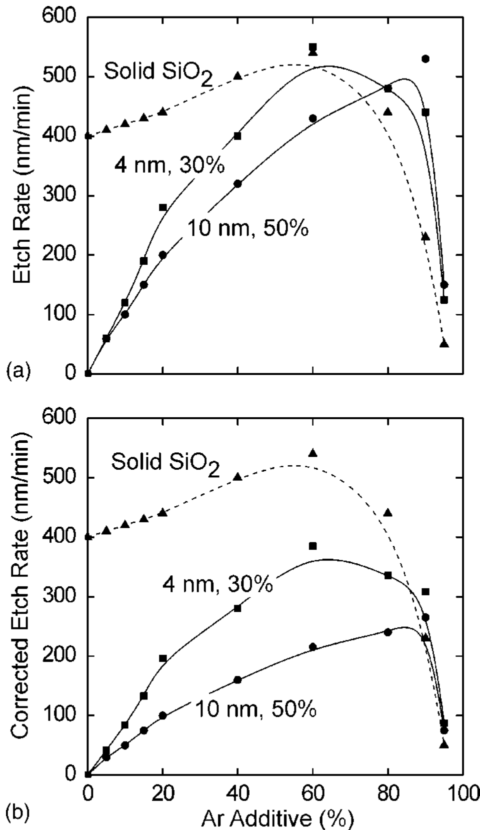

FIG. 5. Rates for blanket etching of solid SiO_2 and porous SiO_2 as a function of Ar mole fraction for the base case with a −120-V self-bias: (a) gross rates and (b) mass corrected rates. Ar addition facilitates etching of porous SiO_2. Larger pores require higher Ar mole fractions to optimize the etch rates.

is ultimately expressed as a probability array for the reaction between the pseudoparticle plasma species and the surface species. When a pseudoparticle hits the surface, a reaction is chosen based on these probability arrays using Monte Carlo techniques. With the selected reaction, the identities of the mesh cells are changed, or cells are added or removed constituting reaction products. Gas phase species evolving from these reactions are tracked as new gas phase pseudoparticles. The mesh used here has 1.7-nm^2 cells, which for SiO_2 represents 4–5 equivalent lattice spacings.

Porous SiO_2 is modeled as being stoichiometric SiO_2 with vacuum pores. The pore locations are randomly distributed in the numerical mesh used by the MCFPM. The pore radii are chosen based on a Gaussian probability distribution

$$p(r) \sim \exp\{-[(r-r_0)/\Delta r]^2\}, \tag{1}$$

where r is the radius of the incorporated pore, r_0 is the average pore radius, and Δr is the standard deviation. Algorithms were developed to include the capability of creating both closed and interconnected pore networks, though in this work we consider only isolated pores.[15]

The interaction of energetic particles with surface species is determined by their angle and energy of incidence. The algorithms used for these interactions are discussed in Refs. 15 and 16 and are briefly summarized here. The generalized reaction probability for a particle of energy E incident onto a surface at an angle θ from the vertical is[22,23]

$$p(\theta) = p_0\left(\frac{E^n - E_t^n}{E_r^n - E_t^n}\right) f(\theta), \tag{2}$$

where E_t is the threshold energy of the process, E_r is a reference energy, p_0 is the probability for normal incidence at E_r and $f(\theta)$ is the relative probability at angle of incidence θ. In this work, $f(\theta)$ is a semiempirical function, typical of chemically enhanced sputtering with a maximum near $\theta = 60°$.[22,24] This angular dependence is appropriate for the fundamental chemically enhanced sputtering which occurs at the surface or interface between, for example, polymer and underlying SiO_2.[15] Etch yields which peak at normal incidence results from the penetration of activation energy from ions through the overlying polymer.[25]

Reflection of energetic particles from surfaces can be either specular or diffusive. The energy loss is large for diffusive scattering and small for specular.[26] To account for surface roughness on spatial scales not resolved by our model, we specified that a fraction $f_d = 0.25$ was diffusively scattered. The energy of specularly reflected particle was scaled such that forward-scattered particles retain the majority of their energy. The specularly reflected particle energy for incident energy E_I is

$$E_s(\theta) = E_I\left(\frac{E_I - E_c}{E_{ts} - E_c}\right)\left(\frac{\theta - \theta_c}{90° - \theta_c}\right) \tag{3}$$

for $\theta > \theta_c$, $E_c < E_I < E_{ts}$. Particles having $\theta < \theta_c$ or $E_I < E_c$ are said to diffusively scatter. Particles having $E_I > E_{ts}$ are said to

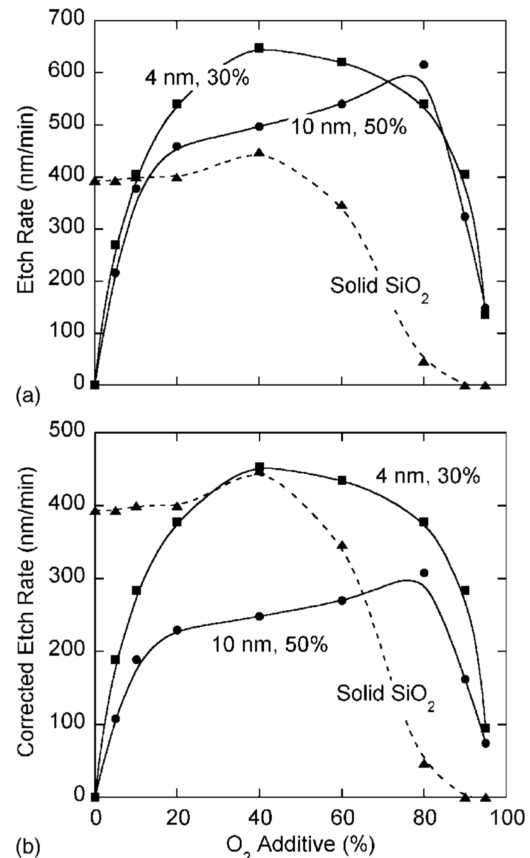

FIG. 6. Rates for blanket etching of solid SiO_2 and porous SiO_2 as functions of O_2 mole fraction for the base case with a −120-V self-bias: (a) gross etch rates and (b) mass corrected rates. Compared to using Ar, less O_2 addition is required to optimize the etch rates in porous SiO_2.

Downloaded 29 Jan 2005 to 129.186.96.224. Redistribution subject to AIP license or copyright, see http://jap.aip.org/jap/copyright.jsp

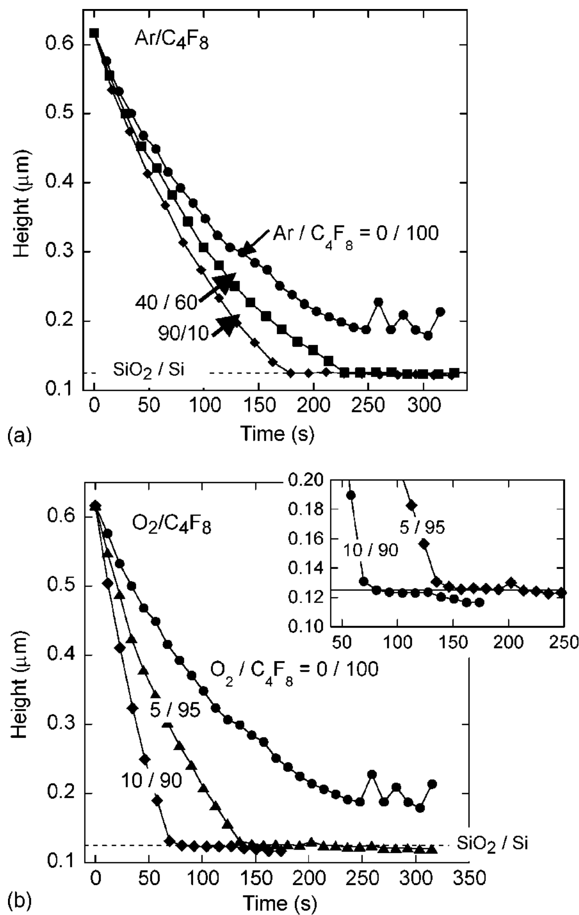

FIG. 7. Heights of the top surface of solid SiO_2 HAR features (including the polymer) as functions of time for the base case conditions (c-C_4F_8, 20 mTorr, 40 sccm, −100-V self-bias) with (a) Ar addition and (b) O_2 addition. The interface between the SiO_2 and the underlying Si is shown by the dashed line. The inset shows etching into the underlying Si. In the absence of additives, an etch stop occurs prior to clearing the feature having an aspect ratio of 5.

retain all of their energy subject to the angular correction. We used $E_{ts}=100$ eV, $E_c=0$ eV, and $\theta_c=60°$. The final reflected energy of the particle is a weighted sum of the specularly reflected energy and diffusively reflected energy.

The surface reaction mechanism used in MCFPM for etching Si and SiO_2 in pure fluorocarbon chemistries such as CHF_3, c-C_4F_8, and C_2F_6 is discussed in Ref. 15. To summarize, etching of SiO_2 proceeds through the deposition of a fluorocarbon polymer overlayer, which is typically $\approx 2-5$ nm and varies with gas chemistry and process conditions.[8] C_xF_y radicals are the precursors to polymer deposition following low-energy ion activation of surface sites.[27] The polymer thickness regulates the delivery of activation energy and reactants to the underlying layers and the polymer-SiO_2 interface. When activated by high-energy ion bombardment [Eq. (2)], the O in SiO_2 reacts with the C and F groups in the polymer to yield volatile etch products such as COF_x and CO_x.[9] Si in the SiO_2 reacts with F in the polymer to produce SiF_x etch products. These processes consume both the polymer and the substrate simultaneously, thereby thinning the polymer layer. In the case of Si, there is no oxygen in the substrate to react with the C and F to produce COF_x etch products. This leads to a thicker polymer film on Si. The end results are lower etch rates for Si and higher etch selectivity between SiO_2 and Si. The polymer layer can also be physically sputtered by energetic ion bombardment.

The reaction mechanism for etching of fluorocarbon polymer in O_2-based plasmas is discussed in Ref. 16 and is summarized here. Little etching of fluorocarbon polymer is typically observed in the absence of there being simultaneous fluxes of oxygen radicals and energetic ions.[28,29] (This differs from hydrocarbon polymers which are often etched in the downstream effluent of oxygen plasmas largely devoid of ions.) In this regard, in the absence of ion bombardment an oxidized layer may be formed on the surface of the polymer which reduces the rates of further reactions.[30] Greer *et al.* observed that etching of fluorocarbon polymer by oxygen plasmas has distinct neutral limited and ion energy limited regimes.[31] Consequently, we modeled the polymer etch mechanism as a two-step process. In the first step, the O radicals bind to the polymer surface forming a layer of activated polymer species which on subsequent energetic ion bombardment releases volatile etch products such as COF_x and CO_x.[16]

A similar etch mechanism was developed for etching of photoresist and which was validated by comparison to ex-

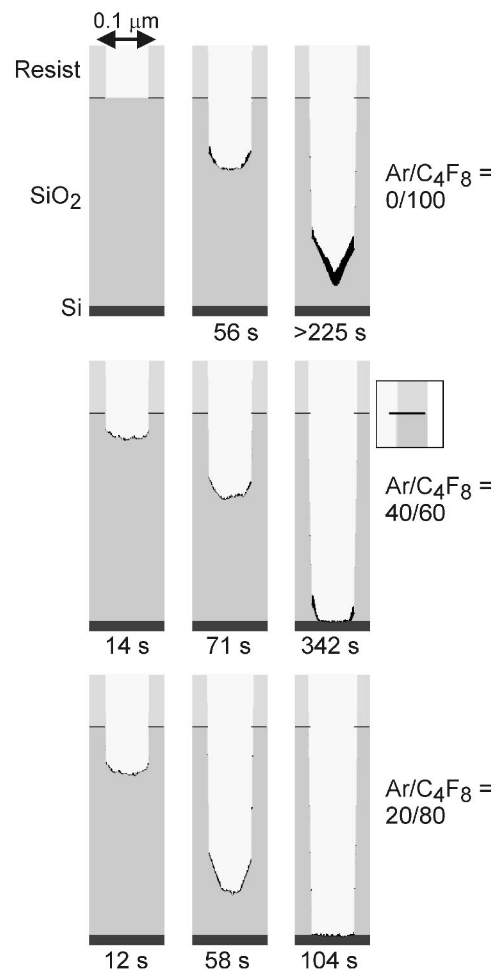

FIG. 8. Selected profiles of HAR features in solid SiO_2 as functions of time and Ar addition for the conditions of Fig. 7. The black material lining the SiO_2 is polymer. The addition of Ar is required to fully clear the feature, though with some loss of critical dimension on the sidewall, as shown by the inset.

Downloaded 29 Jan 2005 to 129.186.96.224. Redistribution subject to AIP license or copyright, see http://jap.aip.org/jap/copyright.jsp

TABLE I. Surface reaction mechanism for resist erosion.

Species	Symbol
Photoresist	R
Activated species	$*$
Ion	I^+
Gas phase species	g
Hot neutral	I_h
Surface species	s

Reaction[a,b]	p_0	E_{th} (eV)	E_r (eV)	n	Ref.
$R_s+O_g \rightarrow R_s^*$	0.01				
$R_s^*+I_g^+ \rightarrow COF_{xg}+I_h$	0.30	100	500	0.8	Eq. (1)
$R_s+I_g^+ \rightarrow CF_{xg}+I_h$	0.20	100	500	0.8	Eq. (1)

[a]Reactions for I_g^+ are generic for all ions. All ions return to the plasma as hot neutrals. Hot neutrals have the same mechanism as ions.
[b]In reactions with no chemical change, the gas phase species are reflected from the surface. These reactions are not shown in the table.

periments performed in a MERIE reactor using a c-C_4F_8/Ar/O_2 gas mixture.[32] The mechanism is summarized in Table I and will be discussed in more detail elsewhere. For the process conditions investigated here having small amounts of oxygen addition with moderate substrate biases and ion fluxes, photoresist erosion is not particularly significant.

III. BLANKET ETCHING OF SOLID SiO_2 AND POROUS SiO_2 IN AN ICP REACTOR

The ICP reactor used for this study is patterned after that used by Li *et al.*[4] The cylindrical chamber is 13 cm in radius and 12 cm in height. The inductive power is supplied through a three-turn antenna coil which sits on a 1-cm-thick quartz window. The wafer is on a substrate 8.5 cm below the quartz window. Gas is injected through a nozzle below the window. A metal ring is used to confine the plasma. The substrate was separately biased at 3.7 MHz to produce a self-dc bias. The base case process conditions are c-C_4F_8 at 20 mTorr pressure, 40-SCCM (standard cubic centimeter per minute) flow rate, and 600-W ICP power at 13.56 MHz.

The gas phase plasma properties for these process conditions and their sensitivity to the parameters of the gas phase reaction mechanism are discussed in Ref. 27. The fluxes of the major ions and neutrals to the substrate are shown in Fig. 1 and listed in Table II for the base case with

TABLE II. Fluxes of selected species to the center of the wafer in a C_4F_8 plasma (600-W ICP, 20 mTorr, 40 sccm, −120-V dc bias).

Species	Flux ($cm^{-2}\,s^{-1}$)
CF_3^+	3.91×10^{14}
CF_2^+	1.35×10^{15}
CF^+	6.17×10^{14}
$C_2F_4^+$	3.75×10^{15}
CF_2	4.08×10^{17}
CF	5.59×10^{16}
F	6.73×10^{15}
C_2F_3	1.46×10^{16}
C_2F_4	3.55×10^{17}

a −120-V dc substrate bias. The dominant neutral fluxes are C_2F_3, C_2F_4, CF_2, CF, and F. The primary electron-impact dissociation reaction of c-C_4F_8 yields C_2F_4. Electron-impact dissociation of C_2F_4 in turn produces CF_2, which is further dissociated to produce CF. The major ion fluxes are CF_2^+, CF^+, CF_3^+, and $C_2F_4^+$. Electron-impact ionization of c-C_4F_8 dominantly produces $C_2F_4^+$ while the smaller ions are generated by ionization of the dissociation products. The large flux of C_2F_3 results from a branching for dissociative ionization of C_2F_4 to $C_2F_3^+$, which upon neutralization on surfaces generates C_2F_3. EADs of CF^+, CF_3^+, and $C_2F_4^+$ for the base case are shown in Fig. 2. The average energy for all the ions is ≈179 eV with an angular spread from the vertical of ≈3°. Heavier ions have narrower EADs in energy, a consequence of their longer crossing time across the sheath and being less affected by collisions.

A comparison of computed etch rates to experiments for blanket etching of solid SiO_2 as a function of the self-generated dc bias for the base case in a c-C_4F_8 plasma is shown in Fig. 3. In accordance with earlier observations for etching of solid SiO_2 in C_2F_6 and CHF_3 plasmas,[15] there is a threshold dc bias for etching, which in this case is ≈40 V. At lower biases and lower ion energies, the rate of polymer deposition is large due to ion activation of surface sites and the rate of polymer sputtering is small, which produces a thicker polymer layer which reduces delivery of activation energy to the substrate. As such, polymer deposition dominates until the threshold bias. Increasing the bias increases ion energies which reduces deposition and increases sputtering, thereby reducing the passivation layer thickness, thus facilitating etching. With further increases in bias, there is a saturation in etch rates due to the reduction of the polymer layer to a submonolayer thickness. Although this increases the delivery of activation energy to the substrate, it also removes the precursors required for SiO_2 etching.

Blanket etch rates for solid SiO_2 as a function of Ar and O_2 addition to c-C_4F_8 for the base case conditions and a dc bias of −100 V are shown in Fig. 4. Increasing the Ar fraction decreases the fluorocarbon mole fraction, thereby reducing the polymerizing fluxes to the wafer, and increases the

Downloaded 29 Jan 2005 to 129.186.96.224. Redistribution subject to AIP license or copyright, see http://jap.aip.org/jap/copyright.jsp

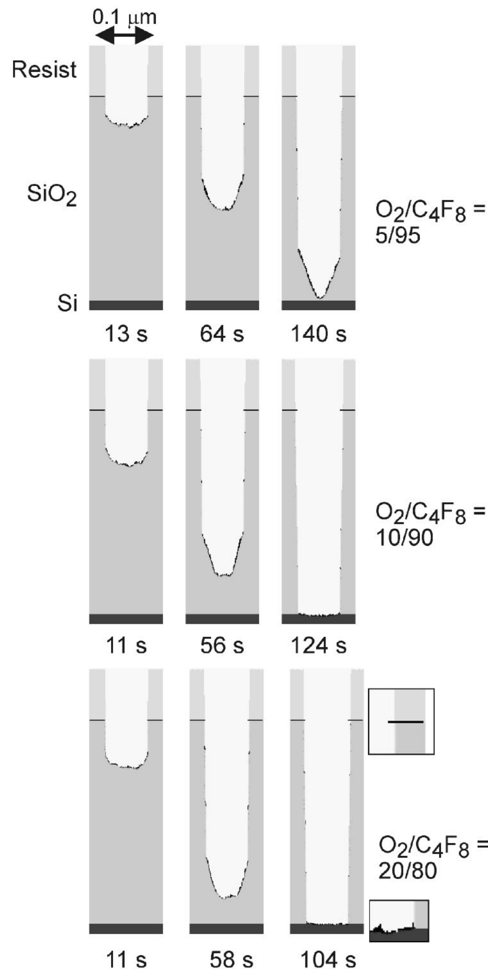

FIG. 9. Selected profiles of HAR features in solid SiO_2 as functions of time and O_2 addition for the conditions of Fig. 7. The black material lining the SiO_2 is polymer. Additions of only small amounts of O_2 are required to fully clear the feature, though with some loss of critical dimension on the sidewall and selectivity to Si, as shown by the insets.

rate of ionization leading to larger ion fluxes. These trends reduce the rate of polymer deposition by fluorocarbon radicals, increases the rate of ion-assisted dissociation at the polymer-wafer interface, and increases the sputtering of the polymer. The end result is that the passivation layer thickness decreases with increasing Ar mole fraction. This has a positive effect on the etch rates as the thinner polymer increases the delivery of activation energy to the surface, producing a maximum etch rate at an Ar mole fraction of ≈ 0.6. At higher Ar fractions the steady-state polymer thickness thins to sub monolayer values and there is an insufficient supply of etch precursors. As a result the etch rate decreases. Comparisons to the experiments of Li *et al.* are favorable.[4]

A similar trend in etch rates for solid SiO_2 occurs with O_2 addition. A maximum in etch rates is obtained with the addition of $\approx 40\%$ O_2, as shown in Fig. 4. Unlike Ar addition, with O_2 addition there is little change in the magnitude of the ion flux and so physical erosion of the polymer does not increase. With O_2 addition, however, O radicals are produced by electron-impact dissociation and these radicals etch the polymer, thereby monotonically reducing its thickness as the O_2 fraction increases. In this parameter space, polymer etching is limited by the availability of O atoms. The O atoms rapidly react with the polymer to form an activated polymer layer, which is then ion sputtered to etch the polymer. This ion-activated process has a lower threshold energy and a higher reaction probability compared to direct sputtering of the polymer or compared to ion-activated etching at the polymer-wafer interface.[16] As a result, the rate of polymer removal is more rapid for a given mole fraction of O_2 addition compared to Ar addition. Less O_2 addition is then required to achieve the optimum polymer thickness and maximum etch rate. Large O_2 mole fractions reduce the polymer thickness to submonolayer values, which essentially terminates etching at O_2 mole fractions of ≈ 0.9, in agreement with the experiments.[4]

In a previous work we found that the scaling laws for etching porous SiO_2 are generally the same as for solid SiO_2. In most cases, porous SiO_2 etches more rapidly than solid SiO_2 due to its inherently lower-mass density. In this regard, we define a corrected etch rate $ER_c = ER(1-p)$, where p is the porosity and ER is the gross etch rate. If there were no

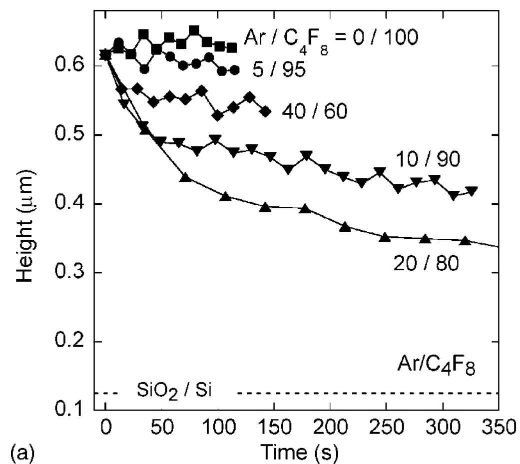

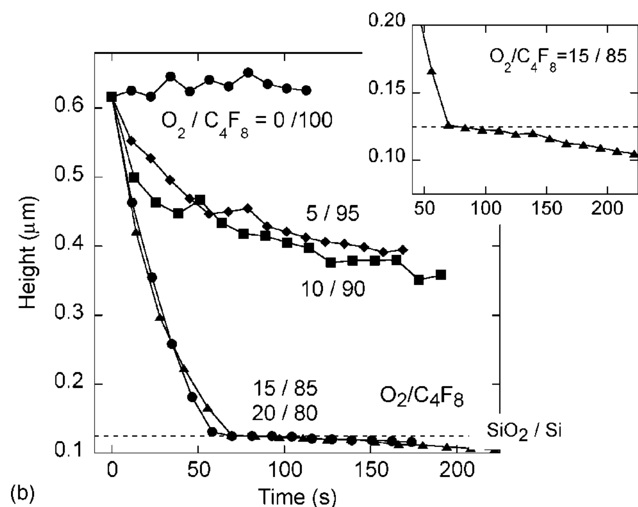

FIG. 10. Heights of the top surface of porous SiO_2 (4 nm, 30% porosity) HAR features (including the polymer) as functions of time for the base case conditions (c-C_4F_8, 20 mTorr, 40 sccm, −100-V self-bias) with (a) Ar addition and (b) O_2 addition. The interface between the SiO_2 and the underlying Si is shown by the dashed line. The inset shows etching into the underlying Si. The feature could not be cleared with Ar addition alone. O_2 addition was able to clear the feature though with some loss of selectivity, as shown by the inset.

Downloaded 29 Jan 2005 to 129.186.96.224. Redistribution subject to AIP license or copyright, see http://jap.aip.org/jap/copyright.jsp

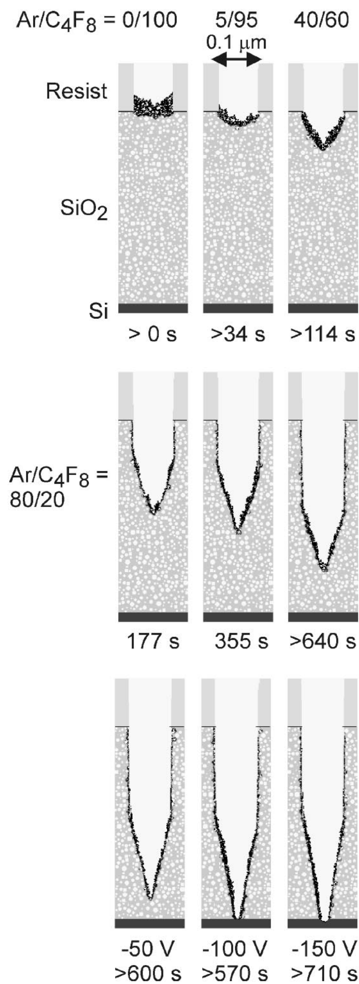

FIG. 11. Selected profiles of HAR features in porous SiO_2 (4 nm, 30%) as functions of time and Ar addition for the conditions of Fig. 10. The black material lining the SiO_2 is polymer. The addition of Ar was not sufficient to clear the feature. Increasing the dc bias (more negative) to increase the ion energies (shown by the lower three frames) averted etch stop though produced tapered profiles.

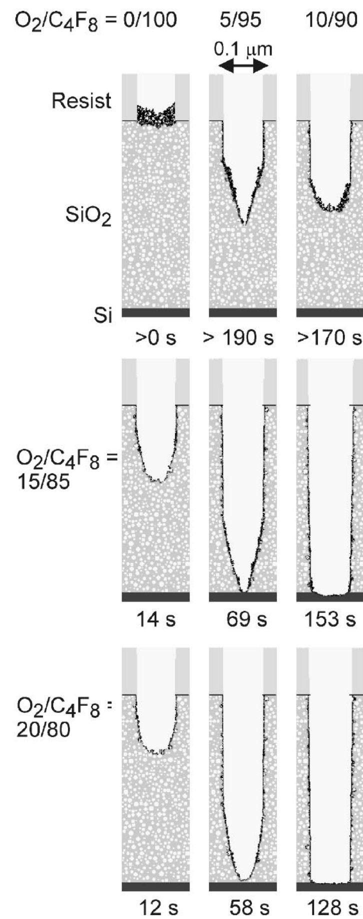

FIG. 12. Selected profiles of HAR features in porous SiO_2 (4 nm, 30%) as functions of time and O_2 addition for the conditions of Fig. 10. The black material lining the SiO_2 is polymer. The addition of $\geqslant 15\%$ O_2 was able to clear the feature, though with some loss of selectivity.

physical or chemical effects due to porous SiO_2, then the ER_c should equal the gross etch rate. The observation is that the filling of pores with polymer can have both positive ($ER_c > ER$) and negative ($ER_c < ER$) consequences depending on the value of L/a (polymer thickness/pore size).[15] When $L/a \lesssim 1$, filling of pores can increase the average polymer thickness at a given site. As a result, porous SiO_2 which has large pores or a large porosity may also have $ER_c < ER$. For sufficiently large pores, even the gross etch rate may decrease below that of solid SiO_2. Conversely, when $L/a \gtrsim 1$, there may be instances when $ER_c > ER$. In these cases, the larger surface area-to-volume ratio afforded by the pores and the more favorable angle of incidence of ions result in a more rapid removal of mass.

Etch rates for two porous SiO_2 blanket films (4-nm pore radius and 30% porosity; and 10-nm pore radius and 50% porosity) as a function of Ar and O_2 addition for the base case conditions with a –120-V bias are shown in Figs. 5 and 6. In pure c-C_4F_8 plasmas, which provide highly polymerizing fluxes, etching occurs for solid SiO_2 but not for the porous SiO_2. The steady-state polymer thickness on SiO_2 in the pure c-C_4F_8 plasma is $\approx 3-5$ nm. Filling of opened pores with polymer produces effective polymer thickness of up to 15 nm, which exceeds the ability for the ions to penetrate through the polymer for these bias conditions. As the Ar addition increases, polymer erosion increases and deposition fluxes decrease, thereby reducing the polymer overlayer, which then enables the porous SiO_2 to begin etching. The etch rate for porous SiO_2 having smaller pores and lower porosity (4 nm, 30%) increases more rapidly with Ar addition as the SiO_2 having larger pores and porosity (10 nm, 50%) is more sensitive to the pore filling effect.[15] The optimum Ar fraction increases as the porosity and pore size increase, an indication that a larger ion flux is required to remove the polymer from the recesses of the porous SiO_2. The etch rates optimize at 60% Ar addition for the 4-nm material and 90% Ar addition for the 10-nm material. For both porous SiO_2 films, the mass corrected etch rates ER_c are smaller than the etch rate of solid SiO_2, except at high Ar fractions. At these mole fractions, the persistence of polymer in the pores is actually advantageous. With solid SiO_2, the polymer would have been reduced to a submonolayer thickness, thereby reducing etch rates. The persistence of polymer in the pores even with high ion fluxes and low polymerizing fluxes enables the etch rate to also persist to larger Ar additions.

Downloaded 29 Jan 2005 to 129.186.96.224. Redistribution subject to AIP license or copyright, see http://jap.aip.org/jap/copyright.jsp

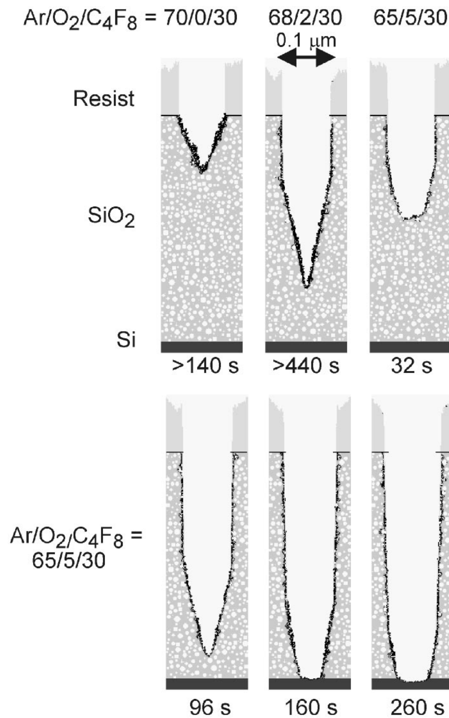

FIG. 13. Selected profiles of HAR features in porous SiO_2 (4 nm, 30%) as functions of time for O_2 addition to Ar/c-C_4F_8. (10 mTorr, 600 W). The black material lining the SiO_2 is polymer. The addition of $\geqslant$5% O_2 was able to clear the feature.

Similar to etching of solid SiO_2, less O_2 addition is required to optimize etch rates and to counter the pore filling effect in porous SiO_2 compared to Ar addition. Etch rates of porous SiO_2 increase significantly with a small O_2 addition, as shown in Fig. 6. In general, a net increase in the overall polymer thickness due to pore filling has a nonlinear effect on the rates of the ion-assisted processes. Since there is a disproportionate delivery of lower activation energy to the inside surfaces of the pores, those processes that benefit from low-energy activation are enhanced. As a result, the neutral-based etching by O radicals is more efficient in removing the polymer from the pores than ion bombardment alone (the mechanism with Ar addition) due to its lower activation energy. As a result, ER_c exceeds the etch rate of solid SiO_2 with only 40% O_2 addition for the 4-nm material. The maximum in etch rate for the 10-nm SiO_2 film occurs with $\approx$80% O_2 addition. This is a result of there being an increased pore filling and thicker polymer layers with larger pores, thereby requiring more O atom etching to counterbalance.

IV. ETCHING OF HIGH ASPECT RATIO FEATURES

To investigate the consequences of these reaction mechanisms on profile evolution, the MCFPM was used to investigate etching of HAR features in solid and porous SiO_2. The features are 0.1 μm wide with an aspect ratio of $\approx$5 over Si. The heights of the features as a function of time for the etching of solid SiO_2 in Ar/c-C_4F_8 and O_2/c-C_4F_8 mixtures are shown in Fig. 7. Selected profiles at different times are shown in Figs. 8 and 9. The dc self-bias is −100 V. Etching of HAR features for these conditions in pure c-C_4F_8 results in an etch stop prior to clearing the feature. The etch rate is initially $\approx$250 nm/min, nearly the same as for blanket etching. As the trench deepens, the etch rate decreases, a process often called aspect-ratio-dependent etching (ARDE).[33] Just prior to stopping, the etch rate slows to $\approx$40 nm/min. In this case, the decrease in the etch rate and eventual etch stop result from an increasing thickness of the polymer. As the trench deepens, the average energy of energetic particles decreases due to reflection of ions from the sidewalls. Polymer removal requires higher-energy particles while polymer deposition is initiated by lower-energy particles. Therefore, as the trench deepens, the likelihood for there being a thicker polymer increases. The grooved appearance of the feature at the etch stop is characteristic of excessive polymerization.

With addition of Ar, the etch rate increases, the magnitude of the ARDE lessens, and the etch stop is averted. Ar addition of at least 50% is required to completely clear the corners of the feature at the Si/SiO_2 interface. For example, the Ar/c-C_4F_8=40/60 case shown in Fig. 8 has a thick polymer layer at the bottom of the trench which prevents ions from clearing the corners. As in the blanket etching examples, the higher rate of sputtering and lower flux of polymerizing radicals which occur with Ar addition result in thinner polymer layers and the ability to avert the etch stop. The residual polymer thickness on the Si is, however, thick enough to maintain selectivity between the SiO_2 and Si. At the same time, the polymer coverage on the sidewalls is reduced, resulting in some loss of critical dimension, as shown by the inset in Fig. 8.

Similar trends are obtained for etching of HAR features in O_2/c-C_4F_8 mixtures. Since polymer removal is now chemically assisted (as opposed to being only physically sputtered in Ar/c-C_4F_8 mixtures), the etch stop obtained in pure c-C_4F_8 due to there being progressively thicker polymer layers as the trench deepens is averted with only small additions of O_2. For example, a plasma sustained in O_2/c-C_4F_8 =5/95 produces a fully cleared feature while still displaying ARDE. (The etch rate decreases by a factor of $\approx$3 from the top to the bottom of the feature.) Increasing the oxygen mole fraction to O_2/c-C_4F_8=10/90 decreases the feature clearing time by a factor of 2 and almost eliminates ARDE. The penalty which is paid are lower selectivity and loss of critical dimension on the sidewalls. With O_2/c-C_4F_8=5/95, there is sufficient polymer to retain selectivity to Si. With increasing fractions of O_2 the selectivity decreases as shown by the slow etching into the Si underlayer.

The heights of the HAR feature as a function of time for etching of porous SiO_2 (4 nm, 30% porosity) in Ar/c-C_4F_8 and O_2/c-C_4F_8 mixtures are shown in Fig. 10. Selected profiles at different times are shown in Figs. 11 and 12. As in the blanket case, pure c-C_4F_8 etching of this HAR feature produces an immediate etch stop. Unlike the blanket etching cases, small additions of Ar did not produce large enhancements in etch performance. With Ar additions up to 40%, etch stops were produced after achieving only nominal etch depths. For an Ar/c-C_4F_8=80/20 mixture, etching at a significantly reduced rate to an aspect ratio of 2–3 was achieved before reaching an etch stop. The causes for this behavior are similar to the trends seen with solid SiO_2, a propensity to emphasize polymerization processes with increasing depth

Downloaded 29 Jan 2005 to 129.186.96.224. Redistribution subject to AIP license or copyright, see http://jap.aip.org/jap/copyright.jsp

while polymer removal processes become less efficient. The thicker polymer layers obtained with porous SiO_2 and the more diffuse reflection of ions from the rougher sidewalls (which reduces ion energies) exacerbate these effects compared to etching solid material. When limited to 20-mTorr $Ar/c\text{-}C_4F_8$ mixtures at 600 W, the feature could not be completely cleared even by increasing the dc bias by 150 V, as shown in Fig. 11. Although the Si interface is reached, the feature is tapered.

As in etching of solid SiO_2, additions of only moderate amounts of oxygen in $O_2/c\text{-}C_4F_8$ mixtures were able to clear the HAR feature in porous SiO_2, as shown in Fig. 12. Unlike solid SiO_2, additions of 5% and 10% O_2 produced an etch stop at an aspect ratio of ≈ 2. Additions of $\geqslant 15\%$ O_2 were required to fully etch the feature. Although this rapid transition between having an etch stop and obtaining a cleared feature is likely exacerbated by the finiteness of our mesh, the transition is nevertheless a sensitive function of the effective polymer layer thickness which in turn depends on O_2 fraction, bias, pore size, and porosity. Again we find a loss in selectivity with O_2 addition due to the thinning polymer layer.

The synergies between polymer deposition and polymer removal processes can be optimized by using $Ar/O_2/c\text{-}C_4F_8$ mixtures. Increasing amounts of Ar increase physical sputtering and activation of high-energy processes whereas addition of O_2 increases rates of chemically based polymer removal. For example, profiles are shown in Fig. 13 for $Ar/O_2/c\text{-}C_4F_8$ mixtures of 70/0/30, 68/2/30, and 65/5/30 at 10 mTorr. Etch stops occur for O_2 fractions of 0% and 2%, however, the feature can be essentially cleared with an O_2 fraction of 5%, a significantly smaller O_2 addition than is required for $O_2/c\text{-}C_4F_8$ mixtures. The dilution of $c\text{-}C_4F_8$ by Ar serves to both reduce the polymerizing radical flux and to increase the ion flux. A small amount of O_2 addition is then able to regulate the polymer thickness to a near optimum value.

V. CONCLUDING REMARKS

Plasma etching of solid and porous blanket SiO_2 films, and HAR features using $Ar/c\text{-}C_4F_8$, $O_2/c\text{-}C_4F_8$, and $Ar/O_2/c\text{-}C_4F_8$ gas mixtures were investigated. With addition of both Ar and O_2 to $c\text{-}C_4F_8$, blanket etching of solid and porous SiO_2 films showed maxima in etch rates which corresponded to obtaining an optimum polymer thickness. Porous SiO_2 films having larger pores required more Ar and O_2 addition to optimize the etch rate. Etch stops in solid SiO_2 HAR features in pure $c\text{-}C_4F_8$ plasmas could, in general, be cleared with O_2 and Ar addition. Etch stops in porous SiO_2 could, in general, not be cleared by Ar addition alone. O_2 addition was required to reduce polymer thickness sufficiently to clear the feature. The tradeoff between etch rate and loss of critical dimension can be optimized by using $Ar/O_2/c\text{-}C_4F_8$ mixtures.

ACKNOWLEDGMENT

This work was supported by the National Science Foundation (CTS03-15353), Semiconductor Research Corporation and Sematech.

[1] K. Miyata, M. Hori, and T. Goto, J. Vac. Sci. Technol. A **15**, 568 (1997).
[2] J. P. Booth, Plasma Sources Sci. Technol. **8**, 249 (1999).
[3] M. Sekine, Appl. Surf. Sci. **192**, 270 (2002).
[4] X. Li, L. Ling, X. Hua, M. Fukasawa, and G. S. Oehrlein, J. Vac. Sci. Technol. A **21**, 284 (2003).
[5] M. Matsui, F. Uchida, M. Kojima, T. Tokunaga, F. Yano, and M. Hasegawa, J. Vac. Sci. Technol. A **20**, 117 (2002).
[6] N. R. Rueger, M. F. Doemling, M. Schaepkens, J. J. Beulens, T. E. F. M. Standaert, and G. S. Oehrlein, J. Vac. Sci. Technol. A **17**, 2492 (1999).
[7] X. Li, X. Hua, L. Ling, G. S. Oehrlein, M. Barela, and H. M. Anderson, J. Vac. Sci. Technol. A **20**, 2052 (2002).
[8] T. E. F. M. Standaert, E. A. Joseph, G. S. Oehrlein, A. Jain, W. N. Gill, P. C. J. Wayner, and J. L. Plawsky, J. Vac. Sci. Technol. A **18**, 2742 (2000).
[9] M. Matsui, T. Tatsumi, and M. Sekine, J. Vac. Sci. Technol. A **19**, 2089 (2001).
[10] G. S. Oehrlein, M. F. Doemling, B. E. E. Kastenmeier, P. J. Matsuo, N. R. Rueger, M. Schaepkens, and T. E. F. M. Standaert, IBM J. Res. Dev. **43**, 181 (1999).
[11] M. Matsui, T. Tatsumi, and M. Sekine, J. Vac. Sci. Technol. A **19**, 1282 (2001).
[12] H. Hayashi *et al.*, J. Vac. Sci. Technol. A **17**, 2557 (1999).
[13] S. Rauf and P. L. G. Ventzek, J. Vac. Sci. Technol. A **20**, 14 (2002).
[14] X. Li, L. Ling, X. Hua, G. S. Oehrlein, Y. Wang, V. Vasenkov, and M. J. Kushner, J. Vac. Sci. Technol. A **22**, 500 (2004).
[15] A. Sankaran and M. J. Kushner, J. Vac. Sci. Technol. A **22**, 1242 (2004).
[16] A. Sankaran, and M. J. Kushner, J. Vac. Sci. Technol. A **22**, 1260 (2004).
[17] R. L. Kinder and M. J. Kushner, J. Vac. Sci. Technol. A **19**, 76 (2001).
[18] R. L. Kinder and M. J. Kushner, J. Appl. Phys. **90**, 3699 (2001).
[19] A. V. Vasenkov, X. Li, G. S. Oehrlein, and M. J. Kushner, J. Vac. Sci. Technol. A **22**, 511 (2004).
[20] J. Lu and M. J. Kushner, J. Vac. Sci. Technol. A **19**, 2652 (2001).
[21] R. J. Hoekstra and M. J. Kushner, J. Vac. Sci. Technol. B **16**, 2102 (1998).
[22] C. C. Cheng, K. V. Guinn, V. M. Donnelly, and I. P. Herman, J. Vac. Sci. Technol. A **12**, 2630 (1994).
[23] C. F. Abrams and D. B. Graves, J. Appl. Phys. **86**, 2263 (1999).
[24] M. Schaepkens, G. S. Oehrlein, C. Hedlund, L. B. Jonsson, and H.-O. Blum, J. Vac. Sci. Technol. A **16**, 3281 (1998).
[25] H. Chae, S. A. Vitale, and H. H. Sawin, J. Vac. Sci. Technol. A **21**, 381 (2003).
[26] B. A. Helmer and D. B. Graves, J. Vac. Sci. Technol. A **17**, 2759 (1999).
[27] T. E. F. M. Standaert, M. Schaepkens, N. R. Rueger, P. G. M. Sebel, G. S. Oehrlein, and J. M. Cook, J. Vac. Sci. Technol. A **16**, 239 (1998).
[28] M. E. Harper, J. J. Cuomo, and H. R. Kaufman, Annu. Rev. Mater. Sci. **13**, 413 (1983).
[29] F. D. Egitto, F. Emmi, R. S. Horwath, and V. Vukanovic, J. Vac. Sci. Technol. B **3**, 893 (1985).
[30] C. Steinbruchel, B. J. Curtis, H. W. Lehmann, and R. Widmer, IEEE Trans. Plasma Sci. **14**, 137 (1986).
[31] F. Greer, L. Van, D. Fraser, J. W. Coburn, and D. B. Graves, J. Vac. Sci. Technol. B **20**, 1901 (2002).
[32] V. Bakshi (private communications).
[33] R. A. Gottscho, C. W. Jurgensen, and D. J. Vitkavage, J. Vac. Sci. Technol. B **10**, 2133 (1992).

Downloaded 29 Jan 2005 to 129.186.96.224. Redistribution subject to AIP license or copyright, see http://jap.aip.org/jap/copyright.jsp